NONLINEAR SOFTWARE PHANTOM FOR CONDUCTIVITY PERTURBATIONS IN ELECTRICAL IMPEDANCE ENDOTOMOGRAPHY

J. Jossinet* and A. Matias*

* National Institute for Health and Medical Research/INSERM U556, Lyon, France

jossinet@lyon.inserm.fr

Abstract: Electrical Impedance Endotomography (EIE) is a modality of Electrical Impedance Tomography (EIT) where the electrodes are located at the surface of a core placed in the middle of the region of interest. The injected currents flow in the medium surrounding the probe. In EIE, the surface bearing the electrodes is known by construction and the explored domain is not limited by a tangible boundary. The purpose of the presented phantom was the calculation of data sets for the development of reconstruction algorithms for EIE. The model is based on image theory. The algorithm calculates the initial value of the voltage difference across a pair of electrodes on an EIE probe and its change in presence of a cylindrical perturbation with no restriction on the conductivity contrast. The model consists of an iterative process of rapid convergence and high accuracy. It was validated by comparison with linear approximation, correlation with experimental data and image reconstruction. This phantom confirmed and explained the finite response of materials frequently used for in vitro data acquisition such as insulating plastic. The model also enabled the quantification of the error resulting from the frequently used linear approximation based on lead field theory.

Introduction

Electrical Impedance Endotomography (EIE) is an imaging method derived from Electrical Impedance Tomography (EIT). The latter has widely been investigated in the last past decades [1, 2]. This imaging technique produces images of electric conductivity inside a body from impedance data collected using surface electrodes successively switched for current injection and voltage sensing. The main advantages of EIT include relatively low cost, ease-to-use, harmlessness, fast data acquisition and sensitivity to small conductivity changes. However, the spatial resolution of EIT is intrinsically limited by the governing equation (second order elliptic differential equation $\nabla.(\sigma\nabla u) = 0$, where σ is the conductivity and u the potential), the small number of measurements (104 linearly independent measurements for 16 electrodes) and the ill-posedness of the inverse problem. The periphery is better sensed than deeper regions, of lower sensitivity [3, 4]. Finally, EIT is not appropriate for accurate imaging of small and deep located organs.

Electrical Impedance Endotomography (EIE) is a modality the authors have developed for impedance imaging in small and deeply located organs, such as prostate [5, 6, 7]. In this modality, the electrodes are located at the surface of an insulating core placed in the middle of the region of interest (Fig. 1). The current injected by the current source flows in the medium surrounding the probe.

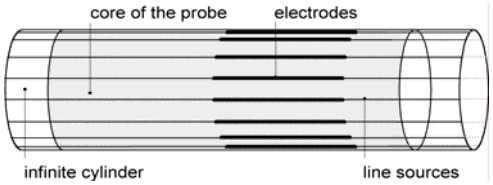

Figure 1: Sketch and 2D model of an EIE probe. The core of the probe is represented by an insulating cylinder of infinite length. The electrodes are represented by infinite line sources at the surface of this cylinder.

Most of concepts studied in EIT [5, 6] are still valid in EIE, but must be revisited [5, 6, 8, 9]. In EIE, the surface bearing the electrodes is known by construction, while it is unknown and variable in EIT. In EIE, there is no tangible external boundary restricting the current lines. It is anticipated that EIE will give rise to new reconstruction algorithms and that their development will require accurate and reliable data sets. The objective of the present software phantom was the calculation of the voltage differences across pairs of sensing electrodes and their changes in presence of a conductivity perturbation.

The present study describes the theory, implementation and evaluation of the 2D software phantom modelling cylindrical perturbations parallel to the axis of the probe of any conductivity value, provided the conductivity is uniform within the perturbation. This model avoids the usual linear approximation that is only valid for small size perturbations and low conductivity contrast. Furthermore, the model has been used to quantify the error resulting from this linear approximation. Two quantities are computed: the first one is the potential difference created by source electrodes located on the probe across a pair of voltage electrodes also located on the probe. The second one is the change in this voltage difference due to the presence of a cylindrical conductivity perturbation.

ISSN: 1727-1983

Modelling the probe

The model of the insulating core of the probe is an infinitely long insulating circular cylinder. Indefinite lines regularly spaced at the outer surface of this cylinder represent the electrodes (Fig. 1). The projection of this model on the calculation plane, of uniform conductivity σ_0, is a circular disk of null conductivity and point sources regularly spaced on the circumference of the disk. It was found convenient to take the radius of this disk as the unit length and its centre as origin of the co-ordinates. The presence of the cylinder creates a boundary condition at it surface. As the cylinder is non-conducting, the current density and the electric field is tangent to the boundary surface. Using this condition, one may demonstrate that, in presence of the cylinder, the external field is the sum of the field of the original source, the field of an image source at the centre of the disk and the field of a source equal to the original one and superimposed to it [5, 6]. As the sum of the currents injected by any set of sourcing electrodes is always equal to zero, the sum of the fields of the central images is also always equal to zero. Hence, only the potential of the images located on the circumference is relevant. Under these conditions, the potential of a source, S, at any point, P, outside the probe is given by (1):

$$v = \frac{I_L}{\pi\sigma_0}\ln\left(|SP|\right) \qquad (1)$$

|SP| denotes the distance of point P to the source and I_L is the current per unit length of the line source. This enabled the calculation of the potential created across a pair of voltage electrodes by source electrodes located on the surface of the probe. The calculation of the change produced in this quantity by the conductivity perturbation was based on the image theory.

Image theory

Image theory is a general method enabling the calculation of the field of electric charges in presence of a surface limiting two half-spaces of different electric or dielectric properties [10, 11].

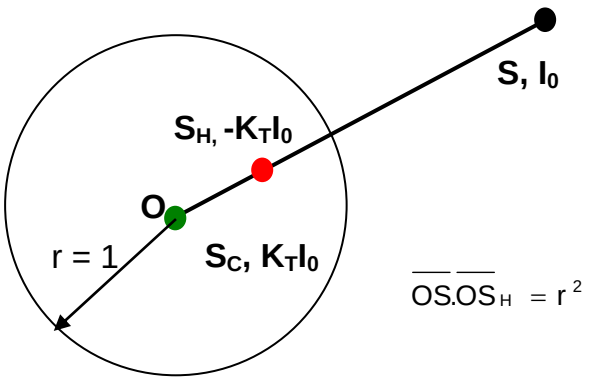

Figure 2: Images S_C and S_H, of a source, S, in a circular perturbation for field calculation outside the disk. The original source and its two images are aligned.

According to this theory, the perturbation produces a change in the potential and electric field of the original source equal to the sum of potential and field, respectively, of two images of the original source with respect to the perturbing disk (Fig. 2). The field and potential inside the perturbation are not useful in this study for the relevant quantity is the potential at electrode located on the probe, consequently outside the perturbation.

The first image, S_C, is located at the centre of the perturbation. The second image, S_H, termed 'harmonic' in this study, is the image of the initial source by the inversion with respect to the circumference of the disk. The central source delivers current $K_T I_0$; the harmonic one, S_H, delivers the current $-K_T I_0$. The quantity K_T, termed the conductivity contrast, is given by (2):

$$K_T = \frac{\sigma_T - \sigma_0}{\sigma_T + \sigma_0} = \frac{c-1}{c+1} \quad \text{with} \quad c = \frac{\sigma_T}{\sigma_0} \qquad (2)$$

The conductivity contrast is equal to -1 for a non conducting material and tends toward 1 for an object of high conductivity. The quantity c was termed the 'conductivity ratio' in the present study. It is interesting to note that the locations of the images are independent of the conductivity contrast and that their magnitudes do not depend on the position of the original sources.

The presence of this disk changes the field of the image sources and results in secondary images in the perturbation. The field of these images is perturbed by the conductivity target, producing new images in the target and secondary images in the core of the probe. This gives rise to an infinite series of images (Fig. 3).

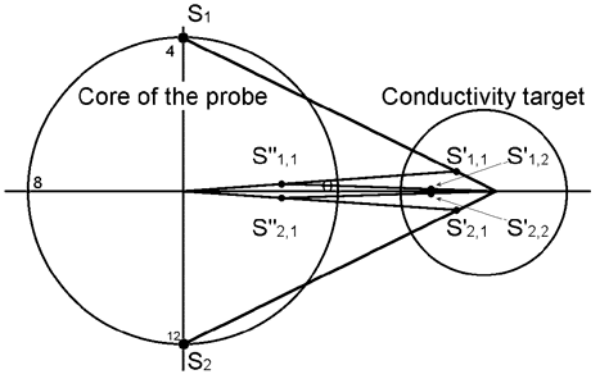

Figure 3: Example showing the successive images in the perturbation and in the core of the probe of initial diametrically opposed sources. In all cases, the images get closer and closer in the perturbation and in the probe, explaining the convergence of the process.

These considerations imply that the calculation of the influence of the conductivity perturbation is an iteration process involving an increasing number of sources. It can be shown, however, that the central images do not play any role in this process, due to the fact that the sum of the current of the original sources is always equal to zero. This property remains true at each iteration step. Consequently, only harmonic images need to be calculated.

ISSN: 1727-1983

Implementation

The programming language was Borland Delphi Professional Programming System. The used floating number format was the non-portable 80-bit, "*extended*" type yielding 18 significant decimal figures. The purpose of the developed software package was the calculation of 1) reference initial voltage ν_{ref}, and 2) changed voltage in presence of the perturbation of conductivity, $\nu_{ref} + \Delta\nu$.

In the present study, the perturbation, also termed the 'conductivity target' and denoted T_C, was characterised by the co-ordinates of its centre, its radius and its conductivity, denoted x_T, y_T, R_T, σ_T respectively.

The voltage sensing electrodes, numbered p and q among the total number, N_E, of electrodes, project in points M_p and M_q on the circumference of the disk modelling the probe in the calculation plane. The projection of a source electrode is denoted S_n and its current is denoted I_n with n varying from to 1 to N_S, the number of sources ($N_S = 2$ for bipolar drive patterns).

The reference data sets consist of the calculated voltage differences across the pair of sensing electrodes, in the initial medium. The generalisation of (1) to a set of sources and a pair of sensing electrodes, p and q, yields the expression of this voltage difference:

$$\nu_{ref}(p,q) = \frac{1}{\pi\sigma_0}\sum_{n=1}^{N_S} I_n \ln\left(\frac{|M_p S_n|}{|M_q S_n|}\right) \qquad (3)$$

Each iteration step consists of two parts: the calculation of the harmonic images in the conductivity target and the calculations of their secondary images in the insulating core of the probe. At each step, k, of the iteration process, the improvement of the voltage change due to the addition of $2\times N_S$ new image sources is denoted $\Delta\nu_k(p,q)$. The contribution of the additional sources is denoted $\delta\nu_k(p,q)$. The actual voltage change, $\Delta\nu_k(p,q)$, at iteration k, is then given by equation (4):

$$\Delta\nu_k(p,q) = \sum_k \delta\nu_k(p,q) \qquad (4)$$

The final value of $\Delta\nu(p,q)$ is the last value of $\Delta\nu_k(p,q)$. Image sources in the conductivity target and in the core of the probe are denoted $S'_{n,k}$ (current $I'_{n,k}$) and $S''_{n,k}$ (current $I''_{n,k}$), respectively.

The initial sources are the N_S current injecting electrodes denoted S_n, with $S_n = S'_{n,0}$. Using the inversion equation given in Fig. 2 with $r = R_T$, the co-ordinates (X_H, Y_H) of the harmonic image in the perturbation conductivity of a source of co-ordinates (x_T, y_T) are given by (5a) and (5b):

$$x_H = x_T + \frac{x_S - x_T}{(x_S - x_T)^2 + (y_S - y_T)^2} R_T^2 \qquad (5a)$$

$$y_H = y_T + \frac{y_S - y_T}{(x_S - x_T)^2 + (y_S - y_T)^2} R_T^2 \qquad (5b)$$

Using (1), the contribution, $\delta\nu_k$, of the new images at iteration k is given by following equation (6):

$$\delta\nu_k(p,q) = -\frac{I_L}{\pi\sigma_0}\sum_{n=1}^{N_S}\left(I'_{n,k}\ln\frac{|M_p S'_{n,k}|}{|M_q S'_{n,k}|} + I''_{n,k}\ln\frac{|M_p S''_{n,k}|}{|M_q S''_{n,k}|}\right)$$

Convergence

The quantification of convergence required the definition of two coefficients. The first coefficient, denoted $\gamma_k(p,q)$, characterises the improvement of the calculated value at iteration k. This dimensionless coefficient is defined by equation (7):

$$\gamma_k(p,q) = \left|\frac{\delta\nu_k(p,q)}{\sum_{\lambda=1}^{\lambda=k}\delta\nu_\lambda(p,q)}\right|. \qquad (7)$$

The second coefficient, denoted Γ_k, is the sum of $\gamma_k(p,q)$ calculated, at a given iteration, for all the sensing pairs (p,q) of adjacent electrodes distinct from the source electrodes. Γ_k is given by (8)

$$\Gamma_k = \sum_{p,q}\gamma_k(p,q) \qquad (8)$$

Coefficients Γ_k and γ_k play complementary roles. Coefficient $\gamma_k(p,q)$ is suitable to stop iteration in practical computations, while Γ_k, the overall incremental improvement of $\Delta\nu_k(p,q)$, has been used in convergence studies (Fig. 4), as it averages possible residual variability of γ_k against different pairs of sensing electrodes. The other factors affecting convergence are the features of the target (conductivity contrast, location and size) and the locations of source electrodes.

The study of convergence was achieved varying target's size (R_{T1}= 0.5, R_{T2} = 0.2), conductivity contrast (± 0.33, ± 67, ± 82, and ± 1) and distance to the origin ($x_T = 2$ and $x_T = 4$, $y_T = 0$). The source electrodes, numbered S_4 and S_{12}, were diametrically opposed on axis Oy. This electrode pattern was chosen as it represented the worst-case initial conditions. Fig. 4 shows the plots of γ_k against iteration number, k. For these calculations, the iterations stopped for $\gamma_k \le 10^{-12}$.

Fig. 4 shows that, under the present conditions calculation accuracy is between 10^{-12} and 10^{-17}, the number of iterations to reach the final value is between 5 and 10 and the convergence speed depends on perturbation's size and distance to the probe.

Convergence is faster for small and/or distant objects and for decreasing $|K_T|$. The interpretation of the latter feature is the need for more image sources to account for stronger perturbation caused by big and/or high contrast objects. Fig. 4 also shows that K_T affects the convergence by roughly 2 to 4 orders of magnitude. As a result, the accuracy may vary between 10^{-13} to 10^{-17}. In all cases, this is better than the resolution of the floating numbers formats in usual software packages.

ISSN: 1727-1983

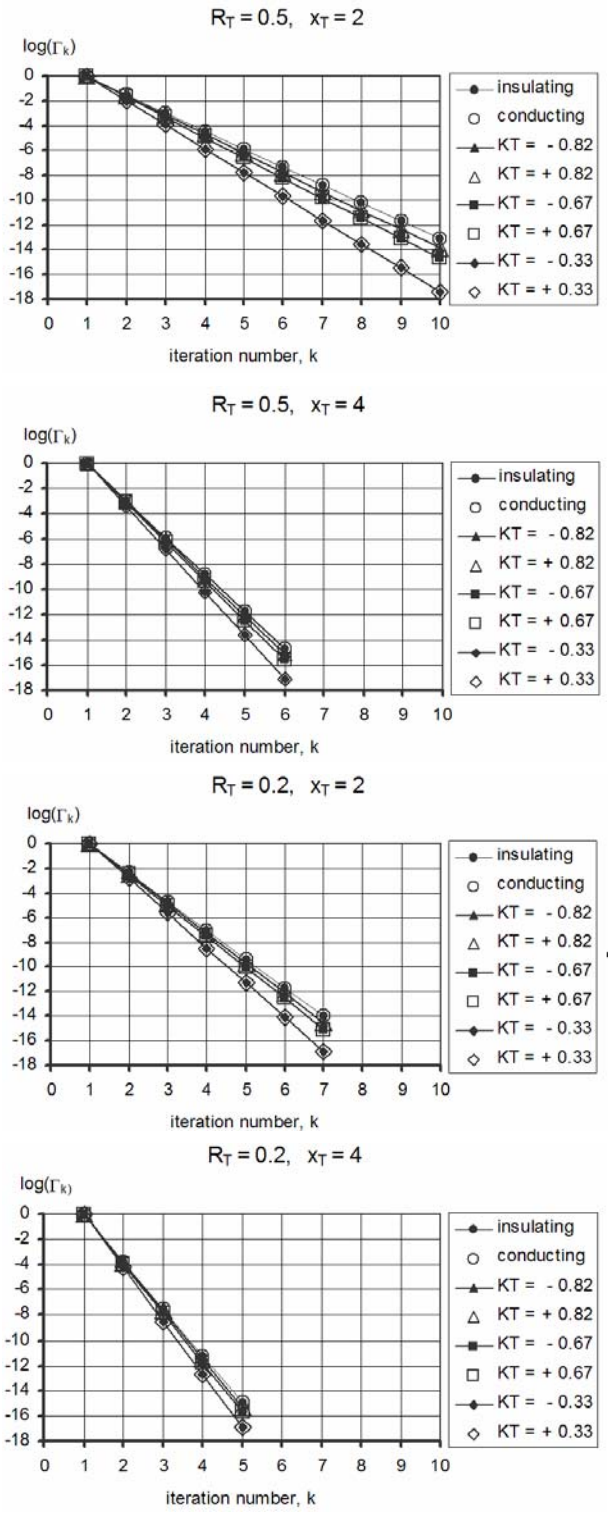

Figure 4: Relative error against iteration number for two perturbation sizes ($R_T = 0.5$, $R_T = 0.2$) and two locations on the Ox axis ($X_T = 2$, $X_T = 4$) for varying conductivity contrast K_T.

The sign of the conductivity contrast is responsible for dissymmetry in convergence for objects of same locations and size, but with opposite values of K_T (Table I). This effect, hardly visible in Fig. 4, is due to the inversion of polarity of new images at each iteration step. This inversion only occurs for positive K_T (objects more conducting that the background). For negative K_T, the denominator is the sum of all positive increments; its magnitude increases at each iteration and is larger than the sum of increments having equal absolute values and alternating signs.

Table I: Influence of the conductivity contrast at successive iteration steps (same data as in Fig. 4).

	1	2	5	10
insulating	1	2.97E-02	1.31E-06	7.35E-14
K_T = -0.82	1	2.45E-02	5.92E-07	1.21E-14
K_T = -0.67	1	2.00E-02	2.62E-07	1.93E-15
K_T = -0.33	1	1.01E-02	1.66E-08	3.82E-18
K_T = +0.33	1	1.04E-02	1.70E-08	3.91E-18
K_T = +0.67	1	2.09E-02	2.75E-07	2.02E-15
K_T = +0.82	1	2.58E-02	6.26E-07	1.28E-14
conducting	1	3.18E-02	1.41E-06	7.86E-14

Validation

The validation of the software phantom was achieved by comparison with data sets from linear approximation, correlation with experimental data and image reconstruction. The lead field theory yields a linear approximation for the calculation of the change in the measured impedance due to a conductivity change [12]. The lead field is the electric field produces by electrodes injecting a unit current. In this approximation, the change in the measured voltage when the conductivity of a given element change by a slight quantity, $\Delta\sigma = \sigma_T - \sigma_0$, is proportional to the integral over this element of the product of the conductivity change by the dot product of lead fields of the source and sense electrodes [12]. This general statement applies under certain conditions not described here but compatible with impedance imaging in general and the present study in particular [6, 12]. Two values of the voltage change produced by a conductivity target were calculated: one using the present model and one based on the lead field approach. The sources were diametrically opposed (#4,#12) and the voltage electrodes were adjacent (#0,#1). For the linear approximation (lead field theory), the conductivity target was covered by a circular Cartesian mesh of 128 pixels in diameter. The results of the comparison are summarised in Table II and Table III.

Table II: Ratio (model/lead field) of the voltage change for varying distance on Ox axis and constant target size $R_T = 0.2$ for varying conductivity ratio.

	c=1.001	c=1.01	c=1.1	c=1.2	c=1.5	c=2.0
2.0	0.9995	0.9950	0.9521	0.9087	0.7992	0.6657
2.5	0.9995	0.9950	0.9523	0.9089	0.7997	0.6664
3.à	0.9995	0.9950	0.9524	0.9090	0.7999	0.6666
3.5	0.9995	0.9951	0.9524	0.9091	0.7999	0.6666
4.0	0.9995	0.9951	0.9524	0.9091	0.8000	0.6667
4.5	0.9995	0.9951	0.9524	0.9091	0.8000	0.6667
5.0	0.9995	0.9951	0.9524	0.9091	0.8000	0.6667
5.5	0.9995	0.9951	0.9524	0.9091	0.8000	0.6667
6.0	0.9995	0.9951	0.9524	0.9091	0.8000	0.6667

ISSN: 1727-1983

Table III: Same as in Table II with varying target size and constant target location ($x_T = 4$, $y_T = 0$).

R_T	c=1.001	c=1.01	c=1.1	c=1.2	c=1.5	c=2.0
0.01	0.9995	0.9951	0.9524	0.9091	0.8000	0.6667
0.02	0.9995	0.9951	0.9524	0.9091	0.8000	0.6667
0.05	0.9995	0.9951	0.9524	0.9091	0.8000	0.6667
0.10	0.9995	0.9951	0.9524	0.9091	0.8000	0.6667
0.20	0.9995	0.9951	0.9524	0.9091	0.8000	0.6667
0.30	0.9995	0.9950	0.9524	0.9091	0.7999	0.6666
0.40	0.9995	0.9950	0.9523	0.9090	0.7999	0.6665
0.50	0.9995	0.9950	0.9523	0.9090	0.7998	0.6664

The agreement between the two methods is overall very good and better for conductivity ratio, c, tending towards unity (conductivity contrast K_T tending towards zero). The calculated values are practically independent of target location. The influence of target size is small. These findings were useful for the comparison with linear approximation (cf. section 'Generalisation' below). The influence of geometry on convergence can be understood considering Fig. 3.

The first influencing factor is the decrease of the angular distance between sources of opposite polarities at each iteration step. The initial angle depends on the relative locations of the source and the perturbation. The arrangement of Fig. 3, where the object is centred on electrodes' axis of symmetry and the distance between source electrodes at its largest possible value, is the worst-case situation for this factor.

The second influencing factor results from the properties of inversion with respect to a circle. The images of sources located outside the circle are located inside the inversion circle. This applies to the conductivity target and the core of the probe. It can easily be seen that the linear distance between successive images decreases at each iteration step. This effect is obviously stronger for small and distant targets, hence improving the convergence with respect to large perturbations located near the probe, especially for large intervals between sources.

The software phantom was used to simulate data corresponding to real perturbations for experimental data collection (PVC rod immersed in tap water, $\sigma_T = 0$, $\sigma_0 = 0.039$ S/m, $K_T = 1$). The drive pattern was fan3 (208 measurements), the injected current 1 mA_{pp} at 8 kHz and the diameter of the probe 50 mm. The example data in Fig. 5 correspond to a PVC rod 16m in diameter [Jossinet, 2002]. The correlation coefficient ($R^2 = 0.96$) confirms the good agreement between experimental and calculated values.

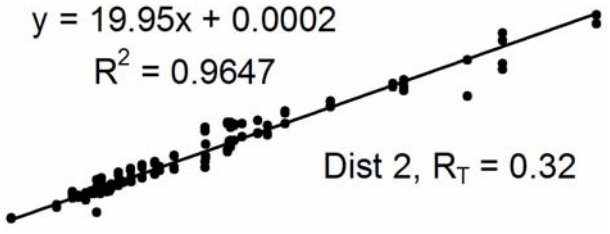

Figure 5: Experimental data against calculated values.

The validity of the calculated values was also verified using the reconstruction algorithm used for the reconstruction of experimental data (solving the normal equation using Tikhonov regularisation). The image corresponding to the example data used in Fig. 5 illustrates the absence of any abnormal feature in the calculated data (Fig. 6).

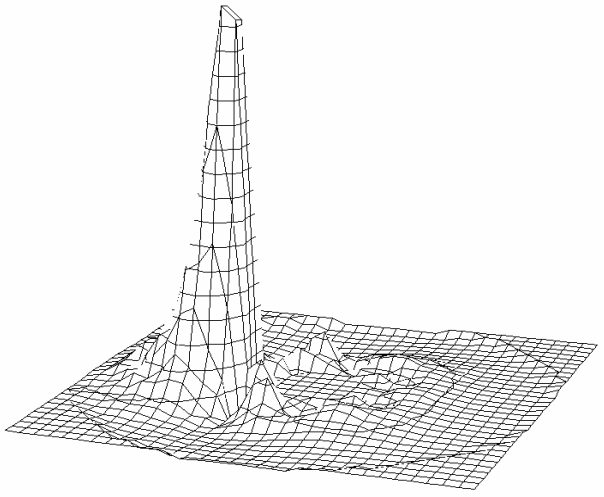

Figure 6: Image reconstructed from simulated data.

Generalisation

The above results show that the present nonlinear model is in agreement with the linear approximation under the validity conditions of the latter and that the nonlinear model is applicable even if these conditions are not met. This suggested the use of the nonlinear approach could as a reference for the evaluation of the error resulting from the linear approximation. The method consisted in the separation, in the expression of the voltage change produced by a circular conductivity perturbation, of the influence of the conductivity contrast from the geometry factors (electrode pattern, size and location of the perturbation). Relatively simple considerations combining the analytical equations for line sources (e.g. (1), the lead field theory and the findings of the above sections enabled to show that in both methods the voltage change can be approximated by the product of a geometry factor and a conductivity factor. The conductivity factors are denoted Q_{LF} for the linear approach and Q_{NLN} for the proposed non linear model. The expressions of Q_{LF} and Q_{NLN} are given by (6a) and (6b):

$$Q_{LF} = \frac{1}{\sigma_m}(c-1) \qquad (6a)$$

$$Q_{NLN} = \frac{2}{\sigma_m}\frac{c-1}{c+1} = \frac{2}{\sigma_m}K_T \qquad (6b)$$

The normalized plots ($\sigma_m = 1$) of (c-1)/2 and K_T against log(c) show that both methods are similar for small conductivity changes and differ strongly for large conductivity changes (Fig. 7). The quantity (c-1)/2 diverges while K_T tends asymptotically.

ISSN: 1727-1983

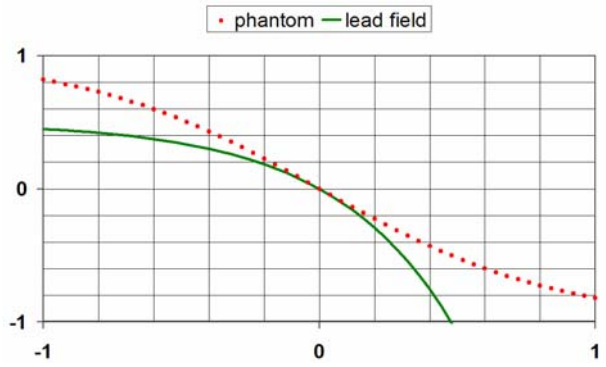

Figure 7: Plots against log(c) of (c-1)/2, representing the linear approximation (solid line), and K_T, representing the response of the nonlinear model (dotted line).

Using (6a) and (6b), the relative error between the linear approximation and the present model is given by (7):

$$(\Delta v_{LF} - \Delta v_{NLN}) / \Delta v_{NLN} = (c-1)/2 \qquad (7)$$

More generally, the plots in Fig. 7 confirm the nonlinearity of the inverse problem in impedance imaging. This plot is agreement with the observation of nonlinear response of the reconstructed conductivity value in EIT [13]. The asymptotical values of K_T for infinite |c| explain the finite response of the insulating rods frequently used for data collection in vitro.

Summary - Conclusion

The propose software phantom enables the simulation of voltage changes sensed by an EIE probe in presence of a circular conductivity perturbation of any conductivity contrast. It overcomes the limitations of the linear approximation. The main results reported in this study are: rapid convergence, good agreement with experimental data and confirmation by image reconstruction. The rapid convergence of the algorithm is explained by the concentration of images of opposite polarities. It reduces the need for physical models of conductivity values differing from zero or tending towards infinity of difficult practical realisation. This software phantom is suitable for the assessment of the intrinsic features of EIE, the design of probes, the specification of hardware systems and the evaluation of algorithms. Possible further improvements include 3D simulation and frequency dependent admittivity.

References

[1] DIJKSTRA A. M., BROWN B. H., LEATHARD A. D., HARRIS N. D., BARBER D. C., and EDBROOKE D. L. (1993): 'Clinical applications of electrical impedance tomography', *J. Med. Eng. Technol.*, **17**, pp. 89-98.

[2] BOONE K., BARBER D., and BROWN B. H. (1997): 'Imaging with electricity: report of the European concerted action on impedance tomography', *J. Med.Eng. Technol.*, **21**, pp. 201-232.

[3] BRECKON W. R., and PIDCOCK M. K. (1987): 'Mathematicals aspects of impedance imaging', *Clin. Phys. Physiol. Meas.*, **8**, pp. A77-A84.

[4] SEAGAR A. D., BARBER D. C., AND BROWN B. H. (1987): 'Theoretical limits to sensitivity and resolution in impedance imaging', *Clin. Phys. Physiol. Meas.*, **8**, pp. A5-A31.

[5] JOSSINET J., MARRY E., and MATIAS A. (2002a) 'Electrical Impedance Endotomography', *Phys. Med. Biol.*, vol. **47**, pp. 2189-2202, 2002.

[6] JOSSINET J., MARRY E., and MATIAS A. (2002b): 'Electrical Impedance Endotomography', *Phys. Med. Biol.*, **47**, pp. 2189-2202.

[7] LEE B. R, ROBERTS W. W., SMITH D. G., KO, H. W., EPSTEIN, J. I., LECKSELL, K., and PARTIN, A. W. (1999): 'Bioimpedance: Novel use of a minimally invasive technique for cancer localization in the intact prostate', *the Prostate*, **39**, pp. 213-218.

[8] JOSSINET J., and DESSEUX A. (2004): 'Electrical Impedance Endotomography: sensitivity distribution against bipolar current patterns', *Physiol. Meas.*, **25**, pp. 355-364.

[9] MOLEBNY V., JOSSINET J., SKIPA, O., and SPUTAI S. (1998): 'I.I.T. Inverse Impedance Tomography: Modelling contrast sensitivity', Proc. 10th ICEBI Int. Conf. on Electrical Bio-Impedance, RIU J., ROSELL J., BRAGOS R. and CASAS O., (Publication Office of UPC, 3861, Barcelona), pp. 415-418.

[10] BINNS, K. J., LAWRENSON, P J. and TROWBRIDGE, C. W. (1992): 'Images', in 'The analytical and numerical solution of electric and magnetic field', (John Wiley and Sons., Chichester), pp. 21-42.

[11] HAYT W. H. Jr (1974): 'Conductors, dielectrics and capacitance', in *Engineering Electromagnetics*, (McGraw-Hill, Tokyo), pp. 117-170.

[12] GESELOWITZ D. B., (1971): 'An application of electrocardiographic lead theory to impedance plethysmography', *IEEE Trans. Biomed. Eng.*, **18**, pp. 38-41.

[13] HOLDER D.S., GONZALEZ CORREA C. A., TIDSWELL T., GIBSON A., CUSICK G., and BAYFORD R.H. (1998) 'Assessment and calibration of a low frequency system for electrical impedance tomography (EIT), optimised for use in imaging brain function in ambulant subjects', Proc. 10th ICEBI Int. Conf. on Electrical Bio-Impedance, RIU P. J, ROSELL J., BRAGÓS R., CASAS O., (Publication Office of UPC, 3861, Barcelona), pp. 479-482.

ISSN: 1727-1983